JACS
JOURNAL OF THE AMERICAN CHEMICAL SOCIETY
pubs.acs.org/JACS
Article

# Stereoselective Growth of Small Molecule Patches on Nanoparticles

Jiajing Zhou, Matthew N. Creyer, Amanda Chen, Wonjun Yim, René P. M. Lafleur, Tengyu He, Zhixing Lin, Ming Xu, Pedram Abbasi, Jianfeng Wu, Tod A. Pascal, Frank Caruso, and Jesse V. Jokerst*

Cite This: https://doi.org/10.1021/jacs.1c04272



**ABSTRACT:** Patchy nanoparticles featuring tunable surface domains with spatial and chemical specificity are of fundamental interest, especially for creating three-dimensional (3D) colloidal structures. Guided assembly and regioselective conjugation of polymers have been widely used to manipulate such topography on nanoparticles; however, the processes require presynthesized specialized polymer chains and elaborate assembly conditions. Here, we show how small molecules can form 3D patches in aqueous environments in a single step. The patch features (e.g., size, number, conformation, and stereoselectivity) are modulated by a self-polymerizable aromatic dithiol and comixed ligands, which indicates an autonomous assembly mechanism involving covalent polymerization and supramolecular assembly. Moreover, this method is independent of the underlying nanoparticle material and dimension, offering a streamlined and powerful toolset to design heterogeneous patches on the nanoscale.

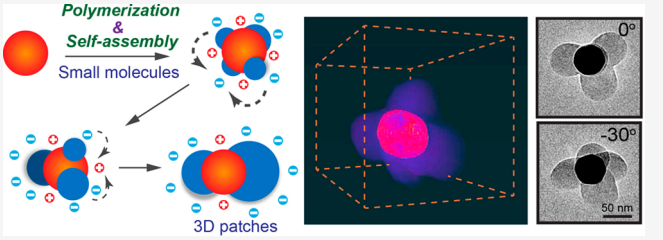




## INTRODUCTION

Surface patterned colloids with anisotropic patches offer fascinating potential in photonics, electronics, biomedicine, and environmental applications as well as important insights into the building blocks of the natural world.[1−5] Current strategies for patchy architectures on micro- and macro-sized colloids include emulsion polymerization, microcontact printing, and glancing angle deposition,[6−9] but the ability to precisely deposit patches on a nanoparticle substrate has been elusive. Although self-assembled monolayers via the segregation of small molecules on nanoparticles can afford multiple "thin" patch modes,[10−12] they lack high-fidelity morphology for further modification or assembling. Therefore, the design of three-dimensional (3D) patches on nanoparticles is envisioned to be a critical step for generating complex and programmable nanostructures toward emerging applications.

Until now, such 3D patchy nanosystems with topographic valence have mainly been obtained through the guided assembly and regioselective conjugation of polymers.[13−17] For example, amphiphilic poly(styrene)-*b*-poly(acrylic acid) in a binary solvent can assemble into an eccentric patch on a nanoparticle that is premodified with hydrophilic and hydrophobic ligands.[18,19] Alternatively, discrete polymer patches can be obtained on polymer-coated nanoparticles via a decrease in the solvent quality.[13,20] These "grafting-to" approaches necessitate the synthesis of customized polymers and the delicate regulation of solvent systems to initiate the transformation of the polymeric chains into patches on the particles. A versatile "one-step" strategy that allows for stereoselective patches from small molecules has remained a challenge.[21−24] Inspired by biological systems that can direct the bottom-up synthesis of nano- and microscopic structures from simple molecules,[25,26] we hypothesized that soluble small molecules capable of both assembling onto nanoparticles and polymerizing into insoluble chains could be utilized to streamline and expand patch design with high-fidelity.

Here, we validate a small molecule-based strategy to synthesize 3D stereoselective patches on nanoparticles of different sizes, shapes, and compositions in aqueous environments. The size of the patch can be easily modulated by varying the amount of benzene-1,4-dithiol (BDT), which can bind to metal surfaces via thiol-mediated chemistry, self-polymerize into polymerized BDT (pBDT) via disulfide bonds, and form finite-sized supramolecular patches via $\pi-\pi$ interactions on nanoparticles without any external stimuli. Experiments and molecular dynamics (MD) simulations corroborate that the spatial distribution of patches on nanoparticles is determined by ligand segregation of modulating ligands (e.g., thiol-carrying small molecules and nonthiol aromatic dyes) and is agnostic to the nanoparticle surface curvature. Eccentric to concentric designs as well as linear through octahedral structures were easily prepared. An autonomous assembly mechanism is proposed to underpin this new type of stereoselective patch. The attractive intermolecular forces among pBDT and their preferential binding to the

Received: April 24, 2021

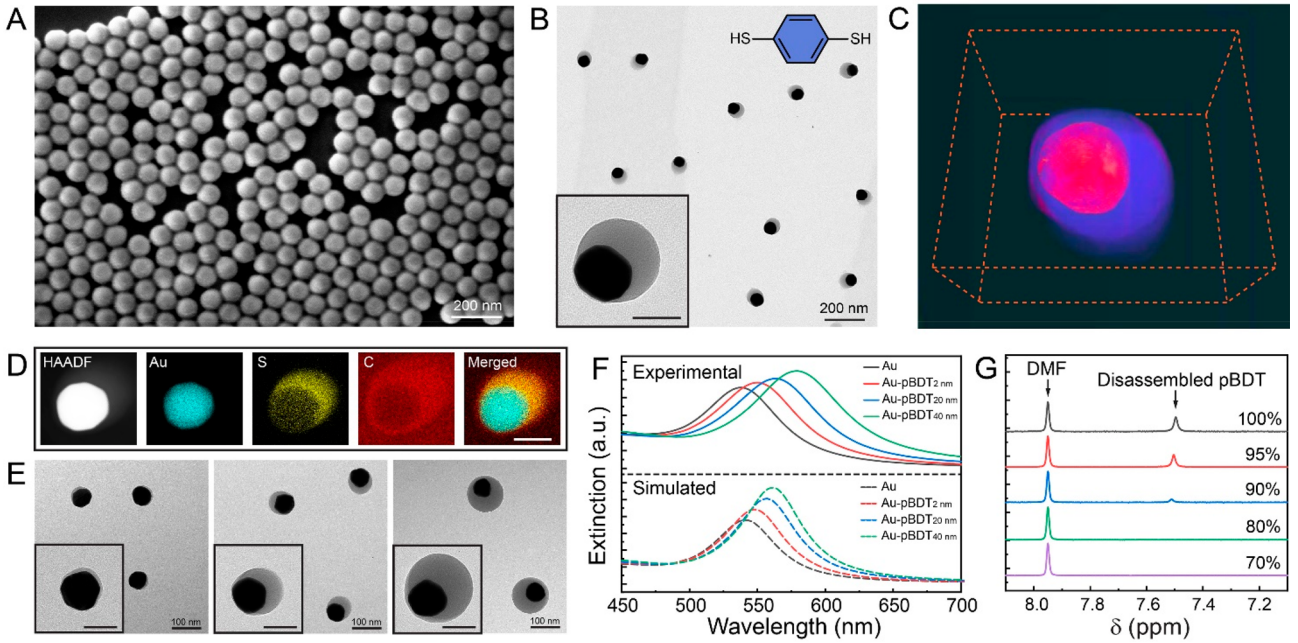


**Figure 1.** Patchy nanoparticles synthesized from small molecules (i.e., BDT). (A and B) Scanning electron microscopy (SEM) and TEM images of the patchy Au-pBDT Janus nanoparticles. (C) Electron tomography reconstruction image of Au-pBDT nanoparticles: Au core (red) and pBDT patch (blue). (D) EDX elemental mapping of Au-pBDT nanoparticles. (E) Patchy Au-pBDT Janus nanoparticles with different patch size, i.e., 2, 20, and 40 nm after increasing the concentration of BDT. Inset scale bars (parts B, D, and E) are 50 nm. (F) Experimental (solid lines) and simulated (dashed lines) extinction of AuNPs and Au-pBDT nanoparticles. (G) $^1$H NMR of pBDT in $(CD_3)_2SO-D_2O$ two-component solvent with different volume ratios of $(CD_3)_2SO$ from 70% (bottom) to 100% (top).

nanoparticle surface are counteracted by the electrostatic repulsion between individual pBDT patches. The resulting patchy nanoparticles present greater opportunities for designing customized colloidal and other complex superstructures.

## RESULTS AND DISCUSSION

To evaluate this approach, we first employed gold nanoparticles (AuNPs, 60 nm) as an example (Figure S1). The AuNPs stabilized by sodium dodecyl sulfate (SDS) were dispersed in bicine buffer (10 mM pH 8.5) followed by the addition of BDT. The thiol moiety of BDT allowed the replacement of the original SDS on the surface of the AuNPs due to the favorable gold−sulfur bonds. Meanwhile, BDT molecules polymerize into pBDT via disulfide bridges,[27] and the hydrophobic backbone of pBDT induces the progressive assembly of pBDT complexes on the surface of AuNPs via $\pi-\pi$ interactions with preabsorbed BDT and/or pBDT (Figures S2 and S3).[28−30] The pBDT-patched AuNPs (Au-pBDT) have a narrow size distribution with no obvious aggregates of pBDT in solution (Figure 1A and Figure S4). Transmission electron microscopy (TEM) and 3D electron tomography reconstruction reveals the anisotropic growth of pBDT patches on AuNPs producing Janus nanoparticles (Figure 1B,C and Movie S1). Energy-dispersive X-ray spectroscopy (EDX) mapping further confirms the patch is composed of C and S indicating the BDT-based patch formulation (Figure 1D). The patch size can be easily tuned from 2 nm to more than 40 nm by adjusting the concentration of BDT molecules (Figure 1E). It is notable that the AuNPs in this study act as substates for patch attachment without showing potential catalytic effects on the polymerization. This is validated by the formation of similar pBDT nanoparticles without adding AuNPs (Figure S4). The anisotropic patch resulted in a polarization-dependent enhancement of an electromagnetic field (Figures S5 and S6) and a redshift in the localized surface plasmon resonance of the Janus nanoparticle (Figure 1F) as validated by experiments and simulations.[31]

The chemical composition of the nanoparticles was examined next. Fourier-transform infrared spectroscopy results show a loss in the $\upsilon_{S-H}$ stretching mode upon disulfide bridging and subsequent patch formation (Figure S7). Janus nanoparticles in deuterium oxide ($D_2O$) exhibit no detectable nuclear magnetic resonance (NMR) signal in the aromatic region due to the densely packed $\pi-\pi$ stacking of pBDT (Figure S7C).[32] In contrast, the intensity of an aromatic proton peak increased with increasing volume ratio of deuterated dimethyl sulfoxide, i.e., $(CD_3)_2SO$ (Figure 1G). This result validates the supramolecular nature of the patches, which can disassemble in organic solvent such as dimethyl sulfoxide (DMSO) and dimethylformamide (DMF) (Figures S8 and S9). Moreover, the supramolecular patch is heat-resistant (e.g., 90 °C for 3 h) and remains intact at high ionic strengths (e.g., 100 mM NaCl or PBS) and extreme pH (pH 2 or 13) (Figures S9 and S10) further confirming their colloidal stability in diverse aqueous conditions.

To study the solution conditions for creating this Janus nanostructure, we investigated the roles of the reactant concentration as well as pH, buffer, surface stabilizer, temperature, and reaction time. The results show that varying the concentration of AuNPs, BDT, or SDS only changes the size of the pBDT patch but not its asymmetrical growth pattern (Figure 1E, Figures S11 and S12, and Table S1). The basic pH (e.g., from pH 7 to >12) facilitates the formation of the patch while acidic media cause aggregation of the nanoparticles and a low yield of Janus nanoparticles (Figure S13). This is likely due to the low solubility of BDT monomers in acid environments.[33]


https://doi.org/10.1021/jacs.1c04272
J. Am. Chem. Soc. XXXX, XXX, XXX−XXX

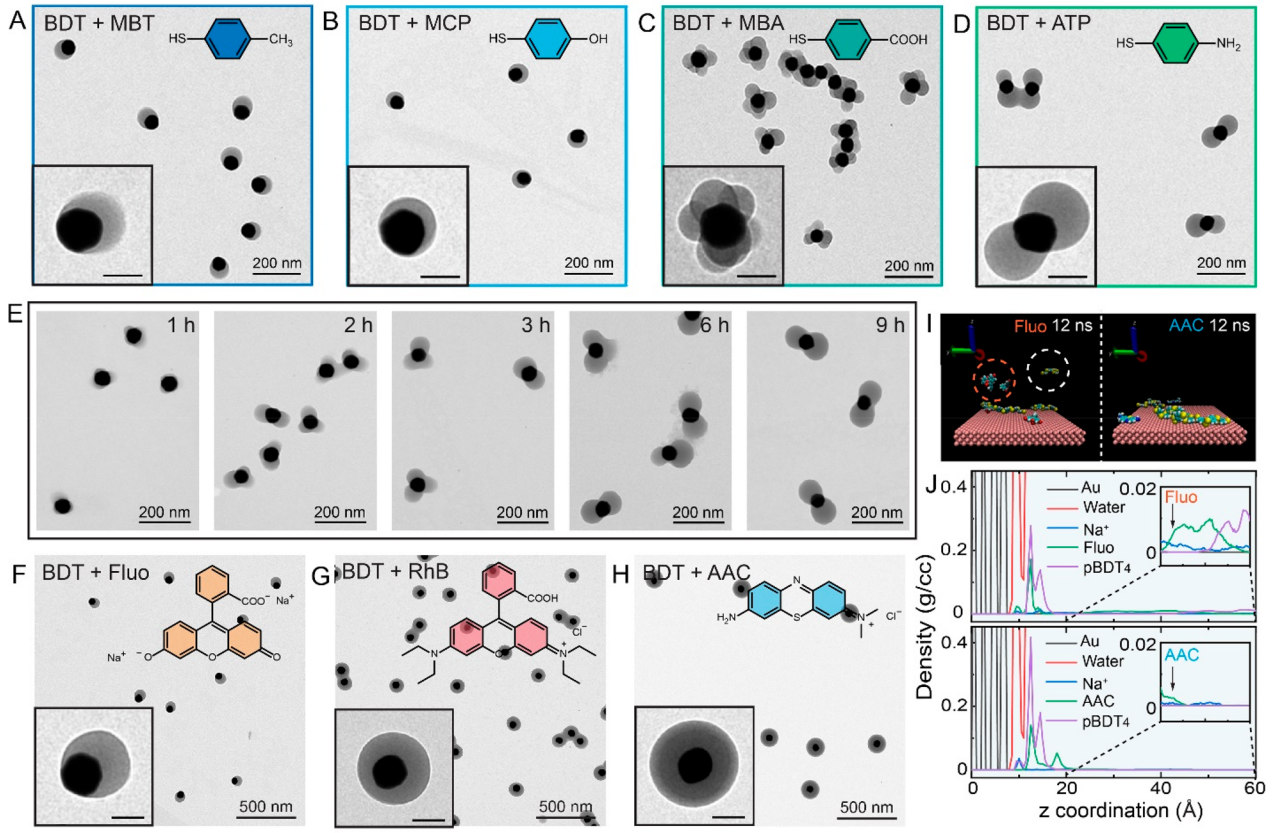


**Figure 2.** Stereoselective tuning of the patch geometry. (A–D) TEM images of the patchy nanoparticles upon the addition of thiol-carrying molecules. Inset TEM images are the close-up image of representative patchy nanoparticles in each scenario; scale bars are 50 nm. (E) Dynamic transition of patch configuration in ATP-guided assembly. (F–H) TEM images of Au-pBDT nanoparticles obtained by adding different dyes. Inset scale bars are 50 nm. (I) The MD snapshot of the tetramer-BDT ($pBDT_4$), and Fluo or AAC on Au substrate (001) at 12 ns at 323 K, 1 atm. Water molecules are not shown for clarity. The white circle highlights the free pBDT in the solution and the orange circle highlights the free Fluo molecules. (J) The mass density-profiles from equilibrium MD simulations. Insets are a magnification of the profile 2 nm from the surface.

The tertiary amine of bicine may interact with gold substrates, and thus we investigated this possible effect using a primary amine-containing buffer (i.e., TRIS buffer) and amine-free media (i.e., NaOH solution). The results show that the amino groups have no contribution to the final morphology due to their weak binding with gold (Figure S14). Other surface ligands (i.e., sodium citrate and sodium dodecylbenzenesulfonate) and reaction temperatures (i.e., 50 °C) can still produce Janus structures (Figures S15 and S16). The time interval between the addition of BDT and Au was investigated showing that Janus nanoparticles of similar patch dimension were obtained within a 1-h window after adding BDT (Figures S17 and S18). Collectively, this approach offers a robust way to synthesize patchy Janus nanoparticles.

Previous atomistic simulations suggested that the competing binding and mobility of multiple thiol-carrying small molecules on a gold surface can induce ligand segregation.[12,34] Therefore, we speculated that introducing a second thiol can alter the ligand distribution and change the symmetry of the pBDT patch patterns. Four BDT analogues were chosen: 4-methylbenzenethiol (MBT), 4-mercaptophenol (MCP), 4-mercaptobenzoic acid (MBA), and 4-aminothiophenol (ATP) (Figure 2A–D). These molecules alone do not produce obvious patches on the surface of the AuNPs (Figure S19). Surprisingly, the 3D morphology of the patches changes drastically from Janus to a dimer or octahedral conformation when the AuNPs were incubated with ATP or MBA for 10 min before adding BDT, respectively (the molar ratio of BDT to the second thiol-carrying molecule is 6:1). In contrast, the addition of MBT or MCP does not change the patch morphology and retains the Janus structure (Figure 2A–D and Figure S20). We reason that the small ligand pattern on AuNPs varies according to the charge and polarity of the additional thiol molecules, which subsequently dictates the 3D configuration of the assembled pBDT patches.

To gain further insight into the assembly process, we investigated the dynamic transition of patch configuration in a BDT-ATP system. A three-patch architecture was dominant at the beginning (<2 h) of the reaction while two linear patches were eventually formed (Figure 2E and Figure S21). It is likely that the electrostatic repulsion between different patches on the confined Au surface increases as patches grow larger and therefore limits their further growth (Figure S22). To overcome this, the existing small patches dissociate and reorganize into a larger patch to lower the surface tension among neighboring patches. This dynamic patch formation suggests an autonomous assembly mechanism that balances surface binding affinity, $\pi-\pi$ interactions among pBDT molecules, and electrostatic repulsion of the polymeric patches (Figure S22C). The resulting patch structures can be maintained at room temperature for more than three months (Figure S23).

Furthermore, the localization of the Au core in patches can be progressively modulated from eccentric to concentric via


https://doi.org/10.1021/jacs.1c04272
J. Am. Chem. Soc. XXXX, XXX, XXX−XXX

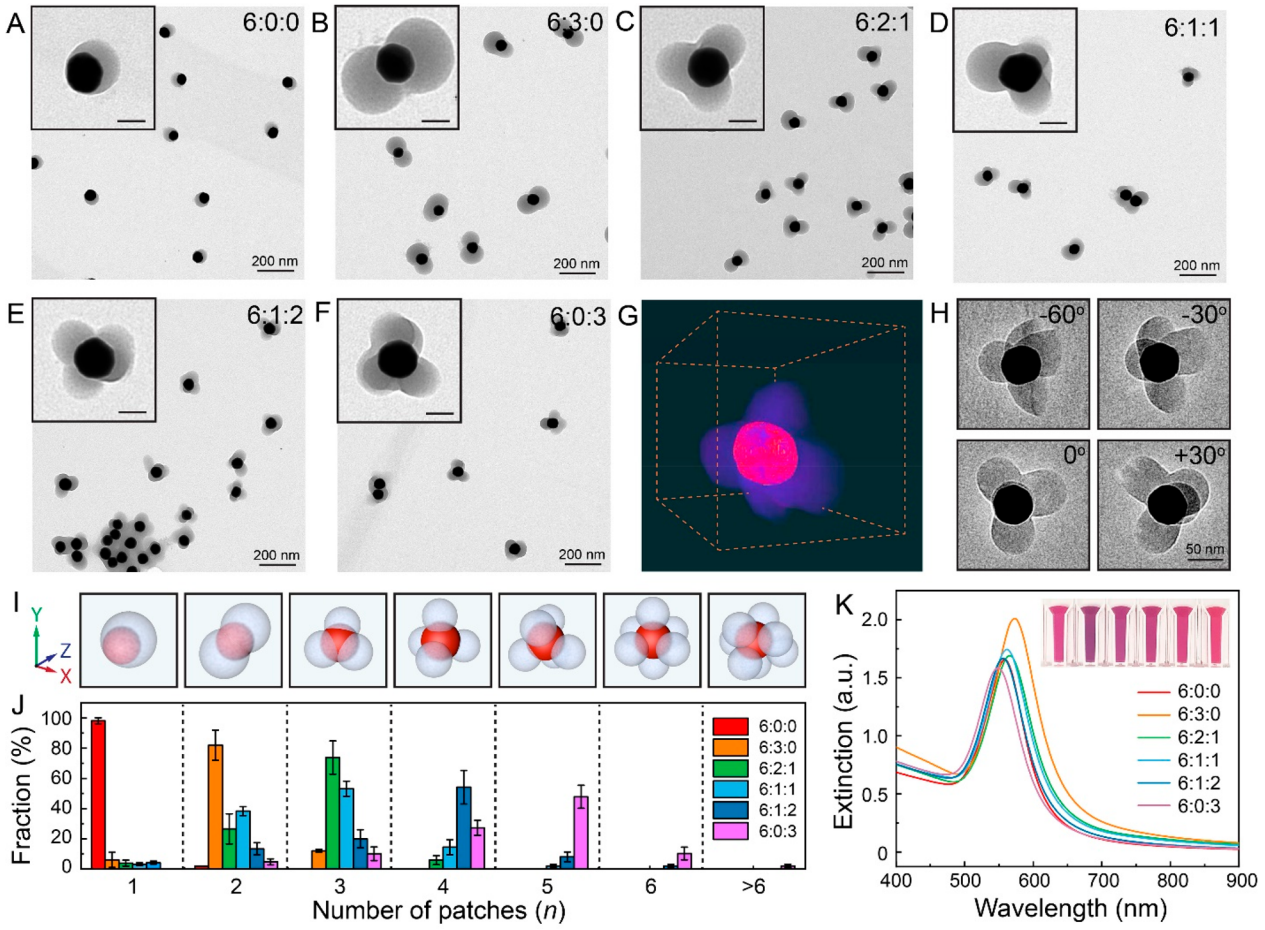


**Figure 3.** Modulating the number of patches using a ternary system. (A–F) TEM images of Au-pBDT patchy nanoparticles by adjusting the ratio of ATP and MBA. The molar ratio of BDT:ATP:MBA is 6:0:0 (A), 6:3:0 (B), 6:2:1 (C), 6:1:1 (D), 6:1:2 (E), and 6:0:3 (F). Inset: scale bar is 50 nm. (G, H) 3D electron tomography reconstruction of a tetrahedral Au-pBDT nanoparticle and corresponding TEM images at different tilting angles. (I) Schematic illustration of different patchy nanoparticles. (J) Population distribution of nanoparticles with different patch numbers in each stoichiometric ratio. The error bars represent the standard deviations: 50 particles were analyzed, and each experiment was run in triplicate. (K) UV–vis spectra and photography of Au-pBDT patchy nanoparticles with differing ligand ratios.

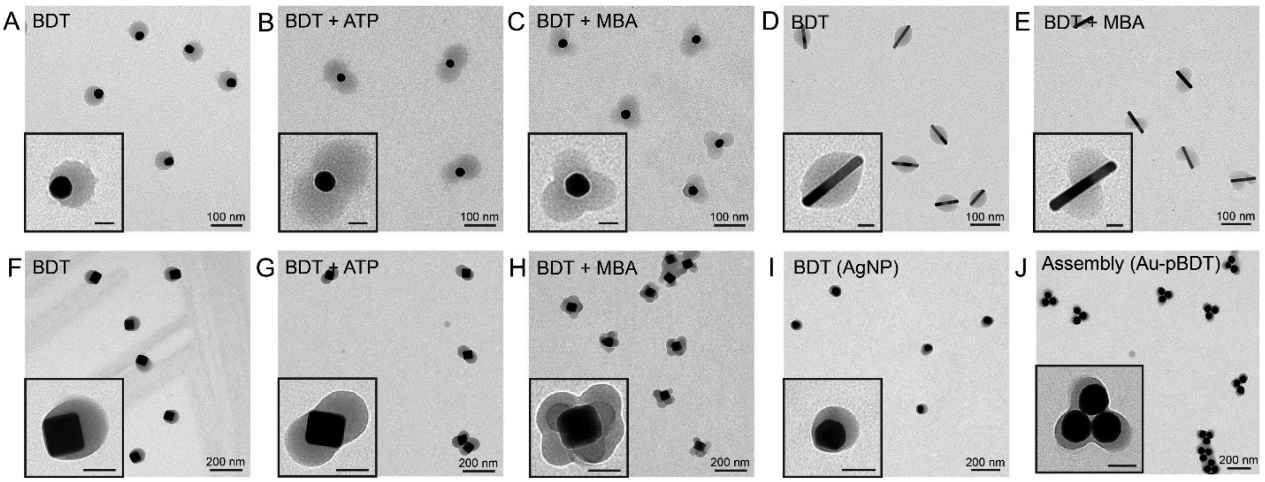


**Figure 4.** Generality of BDT-mediated patch design. (A–C) TEM images of tunable patches on 20 nm AuNPs. (D and E) TEM images of tunable patches on AuNRs. Insets in parts A–E: scale bars are 20 nm. (F–H) TEM images of tunable patches on 60 nm AuNCs. (I) TEM images of patches on AgNPs. (J) Trimer-shaped hierarchical assembly with Au-pBDT. Insets in parts F–J: scale bars are 50 nm.

nonthiol aromatic dye additives (Figure 2F–H and Figure S24). While negatively charged fluorescein sodium (Fluo) largely remains the Janus morphology (i.e., eccentric) (Figure 2F), zwitterionic rhodamine B (RhB) at a similar concentration can make AuNPs entirely engulfed in a slightly off-centered patch (Figure 2G). This particle became even more


https://doi.org/10.1021/jacs.1c04272
J. Am. Chem. Soc. XXXX, XXX, XXX–XXX

symmetrical when a positively charged dye (i.e., azure A chloride, AAC) was used (Figure 2H). We confirmed above that the amino groups do not modulate the gold interface in this system (Figure S14), and thus the charge of the dye is expected to be the key influence on the patch morphology. MD simulations further suggest that the positively charged AAC tends to form complexes with pBDT due to electrostatic attraction and therefore reduces the interfacial energy between Au and pBDT for rapid and conformal deposition (Figure 2I,J, Figures S25−S30, and Tables S2−S6).

Control over the number of patches is an important topic especially for investigating colloidal nanoparticles with valence and directional bonding.[35,36] Since tuning of the concentration of the second thiol-carrying molecules did not considerably change the patch morphology (Figure S20), we employed a ternary system to achieve this goal in which a combination of BDT, ATP and MBA were used in tandem. The number of patches obtained per nanoparticle is proportional to the ratio of MBA to ATP (Figure 3A−F). For example, TEM and 3D tomography reconstruction images clearly showed a tetrahedral structure of patchy Au-pBDT nanoparticles obtained with a stoichiometric ratio of 6:1:2 (i.e., BDT:ATP:MBA) (Figure 3G,H, and Movie S2). All of the products show good monodispersity, and the trends of varying ratios for different patch number are further summarized (Figure 3I,J, and Figure S31). For example, 82% of Au-pBDT nanoparticles had two patches at a molar ratio of 6:3:0, and 52% of the nanoparticles had four patches at 6:1:2. UV−vis spectra confirm that there is negligible aggregation in the products indicating the high yield of the patchy nanoparticles (Figure 3K).

The versatility of this patterning strategy was explored for diverse nanoparticles with different sizes, shapes, and compositions. We created similar Janus-, dimer-, and tripod-like patches on 20 nm AuNPs (Figure 4A−C and Figure S32). Stereoselective patches were also obtained on gold nanorods (AuNRs) and gold nanocubes (AuNCs) (Figure 4D−H and Figures S33 and S34). Considering that they all have different surface curvatures and crystal facets but result in the similar patch structure (Figure S35),[37,38] we infer that these structural parameters do not play an important role in this method, which is in stark contrast with previous studies.[13] Indeed, the pBDT approach was also applicable to silver nanoparticles (AgNPs) (Figure 4I and Figure S36) underscoring its utility with a variety of metal nanoparticles. The resulting patchy nanoparticles can be further utilized as building blocks for hierarchical self-assembly (Figure 4J). We ascribe this unique template-free assembly to a steric interlock mechanism, which can direct the patchy nanoparticles into a staggered conformation.[6]

## CONCLUSIONS

Our work demonstrates a "grafting-from" concept harnessing autonomous covalent and supramolecular assembly of BDT molecules. Importantly, off-target patches are very rare due to the thiol-mediated growth. Growth is exquisitely controlled on the nanoparticle surface, eliminating the need for elaborate purification. The synthesis is performed in aqueous conditions and forms patches on multiple nanoparticle geometries underscoring its versatility. This method described here is primarily mediated by surface binding of BDT/pBDT via thiol-mediated chemistry. Therefore, the extension of this strategy to other nonmetallic particle systems (e.g., polymer and silica) is currently limited and may require additional surface engineering.[39] This aim would be worthy of more efforts and is currently ongoing in our group. Combined with available bioorthogonal chemistry and biological recognition (e.g., antigen−antibody interaction, DNA hybridization), we envision that these tunable high-valence patchy nanoparticles will be indispensable in the design of intricate superstructures and further our understanding of bottom-up assembly in natural systems.

## EXPERIMENTAL SECTION

**Synthesis of 60 nm AuNPs.** AuNPs of 60 nm in diameter were prepared using a seeded growth method. For the preparation, AuNPs (seeds) with a diameter of 20 nm were first synthesized. Then, the AuNPs of 20 nm in diameter were used to synthesize AuNPs of 60 nm in diameter. Briefly, 50 mL water was added into a 100 mL round-bottom flask. Then, 2 mL of the seed solution (20 nm AuNPs) and 200 $\mu$L of 0.2 M $NH_2OH{\cdot}HCl$ were added to this flask consecutively. Then, 3 mL of 0.1 wt % $HAuCl_4$ was added dropwise to the solution under vigorous stirring followed by reaction for 30 min at room temperature. A gradual color change from light red to dark red was observed. Finally, the concentration of sodium citrate was adjusted to 1 mM. After being reacted for another 2 h, the nanoparticle dispersion was stored at 4 °C for further use.

**Synthesis of Au-pBDT Patchy Nanoparticles with 60 nm AuNPs.** For a typical synthesis of Au-pBDT nanoparticles, 50 $\mu$L of 60 nm AuNPs and 100 $\mu$L of 0.5 wt % sodium dodecyl sulfate (SDS) were added to 2 mL bicine buffer (pH 8.5, 10 mM). After the mixture was vigorously stirred for 10 min, 60 $\mu$L of BDT solution (2 mg $mL^{-1}$ in DMF) was added to the above solution. The reaction was stirred for 20 h. Then, the resulting patchy nanoparticles were purified by centrifugation (1600 *g*, 10 min) to remove the supernatant. The pellets were resuspended in water for future use.

**Synthesis of Patchy Nanoparticles with a Second Thiol-Carrying Molecules.** To induce the surface ligand segregation on AuNPs, a second thiol-carrying molecule was added into the systems: 4-methylbenzenethiol (MBT), 4-mercaptophenol (MCP), 4-mercaptobenzoic acid (MBA), or 4-aminothiophenol (ATP). To validate if those monothiol molecules will form patches, 50 $\mu$L of AuNPs was added into 2.0 mL of bicine buffer with 100 $\mu$L of 0.5 wt % SDS. After the solution was stirred for 10 min, 60 $\mu$L of the thiol-carrying molecules was added dropwise. The concentration for each stock solution were 1.75 mg $mL^{-1}$ (MBT) 1.74 mg $mL^{-1}$ (MCP), 2.14 mg $mL^{-1}$ (MBA), and 1.76 mg $mL^{-1}$ (ATP), respectively. The products were collected by centrifugation (1600 *g*, 10 min) after 20 h and measured by UV−vis spectrometer and TEM.

The binary ligand systems were then employed to modulate the ligand segregation. In a typical synthesis, 50 $\mu$L of AuNPs was first added to 0.35 mL of water followed by 100 $\mu$L of 0.5 wt % SDS solution. The solution was stirred for 10 min; different amounts of thiol-carrying molecules in DMF (i.e., 1.75 mg $mL^{-1}$ (MBT), 1.74 mg $mL^{-1}$ (MCP), 2.14 mg $mL^{-1}$ (MBA), or 2.14 mg $mL^{-1}$ (ATP)) were added into the above solution. This solution was gently stirred for 10 min, and 60 $\mu$L of BDT solution (2 mg $mL^{-1}$ in DMF) was added. After another 5 min of gentle mixing, 1.5 mL of bicine buffer (pH 8.5, 10 mM) was added dropwise. The reaction was stirred for 20 h. The resulting patchy AuNPs were then purified by centrifugation (1500 *g*, 10 min) to remove the supernatants. The pBDT-patched AuNPs were resuspended in water for future use. The volume of added thiol-carrying molecules solution was adjusted (i.e., 10, 30, and 60 $\mu$L) to investigate the effect of concentration of second ligand for the final patchy morphology.

**Synthesis of Patchy Nanoparticles (60 nm AuNPs) in a Ternary System.** To modulate the number of patches on single AuNP, we concurrently introduced two thiol-carrying molecules (i.e., MBA and ATP) in the system because ATP can induce two patches and MBA can induce more than 5 patches on AuNPs. In a typical synthesis, 50 $\mu$L of AuNPs was first added to 0.35 mL of water followed by 100 $\mu$L of 0.5 wt % SDS solution. The mixture was stirred for 10 min. Meanwhile, MBA (2.14 mg $mL^{-1}$) and ATP (1.76 mg


https://doi.org/10.1021/jacs.1c04272
J. Am. Chem. Soc. XXXX, XXX, XXX−XXX

$mL^{-1}$) were mixed first to prepare the mixed ligand solution (30 $\mu$L). The mixed ligand solution was then added dropwise into the AuNP solution. This mixture was gently stirred for 10 min; 60 $\mu$L of BDT solution (2 mg $mL^{-1}$ in DMF) was added. After another 5 min, 1.5 mL of bicine buffer (pH 8.5, 10 mM) was added dropwise. The reaction was stirred for 20 h. The resulting patchy AuNPs were then purified by centrifugation (1500 *g*, 10 min) to remove the supernatants. The pBDT-patched AuNPs were resuspended in water for future use. We also compared the results with patchy nanoparticles prepared from 60 $\mu$L of a mixed ligand solution (data not shown here), and we found that using 30 $\mu$L of mixed ligand solution can produce uniform morphology and less free pBDT nanoparticles in the solution. The average number of the patches on individual nanoparticles was summarized based on the TEM images of 50 nanoparticles, and the final results were calculated in triplicate batches of particles.

## ■ ASSOCIATED CONTENT

### Supporting Information

The Supporting Information is available free of charge at https://pubs.acs.org/doi/10.1021/jacs.1c04272.

Detailed experimental procedures for different patchy nanoparticles, characterization of patchy nanoparticles, and detailed simulation results (PDF)

Movie of 3D electron tomography reconstruction of a Janus patchy nanoparticle (MP4)

Movie of 3D electron tomography reconstruction of a tetrahedral patchy nanoparticle (MP4)

## ■ AUTHOR INFORMATION


### Corresponding Author

**Jesse V. Jokerst** − *Department of NanoEngineering, Materials Science and Engineering Program, and Department of Radiology, University of California San Diego, La Jolla, California 92093, United States;* orcid.org/0000-0003-2829-6408; Email: jjokerst@eng.ucsd.edu

### Authors

**Jiajing Zhou** − *Department of NanoEngineering, University of California San Diego, La Jolla, California 92093, United States;* orcid.org/0000-0001-5203-4737

**Matthew N. Creyer** − *Department of NanoEngineering, University of California San Diego, La Jolla, California 92093, United States*

**Amanda Chen** − *Department of NanoEngineering and UC San Diego Material Engineering Research and Education Center, University of California San Diego, La Jolla, California 92093, United States;* orcid.org/0000-0002-7358-222X

**Wonjun Yim** − *Materials Science and Engineering Program, University of California San Diego, La Jolla, California 92093, United States;* orcid.org/0000-0002-0242-7898

**René P. M. Lafleur** − *ARC Centre of Excellence in Convergent Bio-Nano Science and Technology, and the Department of Chemical Engineering, The University of Melbourne, Parkville, Victoria 3010, Australia;* orcid.org/0000-0003-0026-3428

**Tengyu He** − *Materials Science and Engineering Program, University of California San Diego, La Jolla, California 92093, United States;* orcid.org/0000-0002-6767-4849

**Zhixing Lin** − *ARC Centre of Excellence in Convergent Bio-Nano Science and Technology, and the Department of Chemical Engineering, The University of Melbourne, Parkville, Victoria 3010, Australia;* orcid.org/0000-0001-9372-3424

**Ming Xu** − *Department of NanoEngineering, University of California San Diego, La Jolla, California 92093, United States;* orcid.org/0000-0002-6998-8462

**Pedram Abbasi** − *Department of NanoEngineering, University of California San Diego, La Jolla, California 92093, United States;* orcid.org/0000-0001-6835-3062

**Jianfeng Wu** − *California Institute for Telecommunications and Information Technology, University of California San Diego, La Jolla, California 92093, United States*

**Tod A. Pascal** − *Department of NanoEngineering, UC San Diego Material Engineering Research and Education Center, and Sustainable Power and Energy Center, University of California San Diego, La Jolla, California 92093, United States;* orcid.org/0000-0003-2096-1143

**Frank Caruso** − *ARC Centre of Excellence in Convergent Bio-Nano Science and Technology, and the Department of Chemical Engineering, The University of Melbourne, Parkville, Victoria 3010, Australia;* orcid.org/0000-0002-0197-497X

Complete contact information is available at: https://pubs.acs.org/10.1021/jacs.1c04272


### Notes

The authors declare no competing financial interest.

## ■ ACKNOWLEDGMENTS

We thank Dr. Y. Cheng, Mr. C. Moore, Dr. Z. Jin, and Dr. H. Duan for helpful discussions. This work was performed in part at the San Diego Nanotechnology Infrastructure (SDNI) of University of California San Diego, a member of the National Nanotechnology Coordinated Infrastructure (NNCI), which is supported by the National Science Foundation (Grant ECCS-1542148). This work was sponsored in part by the UC San Diego Materials Research Science and Engineering Center (UCSD MRSEC), supported by the National Science Foundation (Grant DMR-2011924). This research was conducted and funded by the Australian Research Council Centre of Excellence in Convergent Bio-Nano Science and Technology (project number CE140100036). M.N.C. acknowledges fellowship funding from T32 CA153915. R.P.M.L. acknowledges The Netherlands Organisation for Scientific Research for a Rubicon postdoctoral fellowship (project 019.182EN.034). F.C. acknowledges the award of a National Health and Medical Research Council Senior Principal Research Fellowship (GNT1135806). J.V.J. acknowledges funding from NIH under DP2 HL137187 and NSF 1845683.

## ■ REFERENCES

(1) Groschel, A. H.; Walther, A.; Lobling, T. I.; Schacher, F. H.; Schmalz, H.; Muller, A. H. E. Guided hierarchical co-assembly of soft patchy nanoparticles. *Nature* **2013**, *503* (7475), 247−251.

(2) Yi, C. L.; Liu, H.; Zhang, S. Y.; Yang, Y. Q.; Zhang, Y.; Lu, Z. Y.; Kumacheva, E.; Nie, Z. H. Self-limiting directional nanoparticle bonding governed by reaction stoichiometry. *Science* **2020**, *369* (6509), 1369−1374.

(3) Hermans, T. M.; Broeren, M. A. C.; Gomopoulos, N.; van der Schoot, P.; van Genderen, M. H. P.; Sommerdijk, N. A. J. M.; Fytas, G.; Meijer, E. W. Self-assembly of soft nanoparticles with tunable patchiness. *Nat. Nanotechnol.* **2009**, *4* (11), 721−726.

(4) Du, J. Z.; O'Reilly, R. K. Anisotropic particles with patchy, multicompartment and Janus architectures: Preparation and application. *Chem. Soc. Rev.* **2011**, *40* (5), 2402−2416.
(5) Cho, E. S.; Kim, J.; Tejerina, B.; Hermans, T. M.; Jiang, H.; Nakanishi, H.; Yu, M.; Patashinski, A. Z.; Glotzer, S. C.; Stellacci, F.; Grzybowski, B. A. Ultrasensitive detection of toxic cations through changes in the tunnelling current across films of striped nanoparticles. *Nat. Mater.* **2012**, *11* (11), 978−985.
(6) He, M. X.; Gales, J. P.; Ducrot, E.; Gong, Z.; Yi, G. R.; Sacanna, S.; Pine, D. J. Colloidal diamond. *Nature* **2020**, *585* (7826), 524−529.
(7) He, Y. X.; Eloi, J. C.; Harniman, R. L.; Richardson, R. M.; Whittell, G. R.; Mathers, R. T.; Dove, A. P.; O'Reilly, R. K.; Manners, I. Uniform biodegradable fiber-like micelles and block comicelles via "living" crystallization-driven self-assembly of poly(l-lactide) block copolymers: The importance of reducing unimer self-nucleation via hydrogen bond disruption. *J. Am. Chem. Soc.* **2019**, *141* (48), 19088−19098.
(8) Lamping, S.; Buten, C.; Ravoo, B. J. Functionalization and patterning of self-assembled monolayers and polymer brushes using microcontact chemistry. *Acc. Chem. Res.* **2019**, *52* (5), 1336−1346.
(9) Chen, Q.; Bae, S. C.; Granick, S. Directed self-assembly of a colloidal kagome lattice. *Nature* **2011**, *469* (7330), 381−384.
(10) Jackson, A. M.; Myerson, J. W.; Stellacci, F. Spontaneous assembly of subnanometre-ordered domains in the ligand shell of monolayer-protected nanoparticles. *Nat. Mater.* **2004**, *3* (5), 330−336.
(11) Harkness, K. M.; Balinski, A.; McLean, J. A.; Cliffel, D. E. Nanoscale phase segregation of mixed thiolates on gold nanoparticles. *Angew. Chem., Int. Ed.* **2011**, *50* (45), 10554−10559.
(12) Luo, Z.; Marson, D.; Ong, Q. K.; Loiudice, A.; Kohlbrecher, J.; Radulescu, A.; Krause-Heuer, A.; Darwish, T.; Balog, S.; Buonsanti, R.; Svergun, D. I.; Posocco, P.; Stellacci, F. Quantitative 3D determination of self-assembled structures on nanoparticles using small angle neutron scattering. *Nat. Commun.* **2018**, *9*, 1343.
(13) Choueiri, R. M.; Galati, E.; Therien-Aubin, H.; Klinkova, A.; Larin, E. M.; Querejeta-Fernandez, A.; Han, L. L.; Xin, H. L.; Gang, O.; Zhulina, E. B.; Rubinstein, M.; Kumacheva, E. Surface patterning of nanoparticles with polymer patches. *Nature* **2016**, *538* (7623), 79−83.
(14) Qiu, H. B.; Gao, Y.; Boott, C. E.; Gould, O. E. C.; Harniman, R. L.; Miles, M. J.; Webb, S. E. D.; Winnik, M. A.; Manners, I. Uniform patchy and hollow rectangular platelet micelles from crystallizable polymer blends. *Science* **2016**, *352* (6286), 697−701.
(15) Xiong, Y.; Yang, S. Z.; Tian, Y.; Michelson, A.; Xiang, S. T.; Xin, H. L.; Gang, O. Three-dimensional patterning of nanoparticles by molecular stamping. *ACS Nano* **2020**, *14* (6), 6823−6833.
(16) Kim, Y.; Macfarlane, R. J.; Jones, M. R.; Mirkin, C. A. Transmutable nanoparticles with reconfigurable surface ligands. *Science* **2016**, *351* (6273), 579−582.
(17) Chen, G.; Gibson, K. J.; Liu, D.; Rees, H. C.; Lee, J. H.; Xia, W. W.; Lin, R. Q.; Xin, H. L. L.; Gang, O.; Weizmann, Y. Regioselective surface encoding of nanoparticles for programmable self-assembly. *Nat. Mater.* **2019**, *18* (2), 169−174.
(18) Kim, A.; Zhou, S.; Yao, L. H.; Ni, S.; Luo, B. B.; Sing, C. E.; Chen, Q. Tip-patched nanoprisms from formation of ligand islands. *J. Am. Chem. Soc.* **2019**, *141* (30), 11796−11800.
(19) Wang, Z. X.; He, B. W.; Xu, G. F.; Wang, G. J.; Wang, J. Y.; Feng, Y. H.; Su, D. M.; Chen, B.; Li, H.; Wu, Z. H.; Zhang, H.; Shao, L.; Chen, H. Y. Transformable masks for colloidal nanosynthesis. *Nat. Commun.* **2018**, *9*, 563.
(20) Yang, Y.; Yi, C.; Duan, X.; Wu, Q.; Zhang, Y.; Tao, J.; Dong, W.; Nie, Z. Block-random copolymer-micellization-mediated formation of polymeric patches on gold nanoparticles. *J. Am. Chem. Soc.* **2021**, *143* (13), 5060−5070.
(21) Walther, A.; Muller, A. H. E. Janus particles: Synthesis, self-assembly, physical properties, and applications. *Chem. Rev.* **2013**, *113* (7), 5194−5261.
(22) Wang, B. B.; Li, B.; Zhao, B.; Li, C. Y. Amphiphilic Janus gold nanoparticles via combining "solid-state grafting-to" and "grafting-from" methods. *J. Am. Chem. Soc.* **2008**, *130* (35), 11594−11595.
(23) van Ravensteijn, B. G. P.; Kegel, W. K. Versatile procedure for site-specific grafting of polymer brushes on patchy particles via atom transfer radical polymerization (ATRP). *Polym. Chem.* **2016**, *7* (16), 2858−2869.
(24) Penfold, N. J. W.; Yeow, J.; Boyer, C.; Armes, S. P. Emerging trends in polymerization-induced self-assembly. *ACS Macro Lett.* **2019**, *8* (8), 1029−1054.
(25) Vantomme, G.; Meijer, E. W. The construction of supramolecular systems. *Science* **2019**, *363* (6434), 1396−1397.
(26) Yu, Z. L.; Tantakitti, F.; Yu, T.; Palmer, L. C.; Schatz, G. C.; Stupp, S. I. Simultaneous covalent and noncovalent hybrid polymerizations. *Science* **2016**, *351* (6272), 497−502.
(27) Liu, B.; Pappas, C. G.; Zangrando, E.; Demitri, N.; Chmielewski, P. J.; Otto, S. Complex molecules that fold like proteins can emerge spontaneously. *J. Am. Chem. Soc.* **2019**, *141* (4), 1685−1689.
(28) Zhou, J. J.; Lin, Z. X.; Penna, M.; Pan, S. J.; Ju, Y.; Li, S. Y.; Han, Y. Y.; Chen, J. Q.; Lin, G.; Richardson, J. J.; Yarovsky, I.; Caruso, F. Particle engineering enabled by polyphenol-mediated supramolecular networks. *Nat. Commun.* **2020**, *11* (1), 4804.
(29) Lin, L.; Zhang, Q.; Li, X. Y.; Qiu, M.; Jiang, X.; Jin, W.; Gu, H. C.; Lei, D. Y.; Ye, J. Electron transport across plasmonic molecular nanogaps interrogated with surface-enhanced Raman scattering. *ACS Nano* **2018**, *12* (7), 6492−6503.
(30) Wang, W. T.; Mattoussi, H. Engineering the bio-nano interface using a multifunctional coordinating polymer coating. *Acc. Chem. Res.* **2020**, *53* (6), 1124−1138.
(31) Goldmann, C.; Lazzari, R.; Paquez, X.; Boissiere, C.; Ribot, F.; Sanchez, C.; Chaneac, C.; Portehault, D. Charge transfer at hybrid interfaces: Plasmonics of aromatic thiol-capped gold nanoparticles. *ACS Nano* **2015**, *9* (7), 7572−7582.
(32) Lafleur, R. P. M.; Lou, X. W.; Pavan, G. M.; Palmans, A. R. A.; Meijer, E. W. Consequences of a cosolvent on the structure and molecular dynamics of supramolecular polymers in water. *Chem. Sci.* **2018**, *9* (29), 6199−6209.
(33) Suwandaratne, N.; Hu, J.; Siriwardana, K.; Gadogbe, M.; Zhang, D. M. Evaluation of thiol Raman activities and pK(a) values using internally referenced Raman-based pH titration. *Anal. Chem.* **2016**, *88* (7), 3624−3631.
(34) Ghorai, P. K.; Glotzer, S. C. Atomistic simulation study of striped phase separation in mixed-ligand self-assembled monolayer coated nanoparticles. *J. Phys. Chem. C* **2010**, *114* (45), 19182−19187.
(35) Ejima, H.; Richardson, J. J.; Caruso, F. Multivalent directed assembly of colloidal particles. *Angew. Chem., Int. Ed.* **2013**, *52* (12), 3314−3316.
(36) Rodriguez-Fernandez, D.; Liz-Marzan, L. M. Metallic Janus and patchy particles. *Part. Part. Syst. Char.* **2013**, *30* (1), 46−60.
(37) Murphy, C. J.; Chang, H. H.; Falagan-Lotsch, P.; Gole, M. T.; Hofmann, D. M.; Hoang, K. N. L.; McClain, S. M.; Meyer, S. M.; Turner, J. G.; Unnikrishnan, M.; Wu, M.; Zhang, X.; Zhang, Y. S. Virus-sized gold nanorods: Plasmonic particles for biology. *Acc. Chem. Res.* **2019**, *52* (8), 2124−2135.
(38) Park, J. E.; Lee, Y.; Nam, J. M. Precisely shaped, uniformly formed gold nanocubes with ultrahigh reproducibility in single-particle scattering and surface-enhanced Raman scattering. *Nano Lett.* **2018**, *18* (11), 6475−6482.
(39) Wu, D.; Zhou, J.; Creyer, M. N.; Yim, W.; Chen, Z.; Messersmith, P. B.; Jokerst, J. V. Phenolic-enabled nanotechnology: versatile particle engineering for biomedicine. *Chem. Soc. Rev.* **2021**, *50* (7), 4432−4483.


https://doi.org/10.1021/jacs.1c04272
J. Am. Chem. Soc. XXXX, XXX, XXX−XXX